ACS Photonics
Article
pubs.acs.org/journal/apchd5

Single-Layer Plasmonic Metasurface Half-Wave Plates with Wavelength-Independent Polarization Conversion Angle

Zhaocheng Liu,[†,‡] Zhancheng Li,[†,‡] Zhe Liu,[§] Hua Cheng,[‡] Wenwei Liu,[‡] Chengchun Tang,[§] Changzhi Gu,[§] Junjie Li,[§] Hou-Tong Chen,[‖] Shuqi Chen,[*,‡] and Jianguo Tian[‡]

[‡]The Key Laboratory of Weak Light Nonlinear Photonics, Ministry of Education, School of Physics and TEDA Institute of Applied Physics, Nankai University, Tianjin 300071, China

[§]Beijing National Laboratory for Condensed Matter Physics, Institute of Physics, Chinese Academy of Sciences, P.O. Box 603, Beijing 100190, China

[‖]Center for Integrated Nanotechnologies, Los Alamos National Laboratory, Los Alamos, New Mexico 87545, United States

Supporting Information

ABSTRACT: Manipulation of polarization state is of great fundamental importance and plays a crucial role in modern photonic applications such as optical communication, imaging, and sensing. Metamaterials and metasurfaces have attracted increasing interest in this area because they facilitate designer optical response through engineering the composite subwavelength structures. Here we propose a general methods of designing half-wave plate and demonstrate in the near-infrared wavelength range an optically thin plasmonic metasurface half-wave plates that rotate the polarization direction of the linearly polarized incident light with a high degree of linear polarization. The half-wave plate functionality is realized through arranging the orientation of the nanoantennas to form an appropriate spatial distribution profile, which behave exactly as in classical half-wave plates but over in a wavelength-independent way.

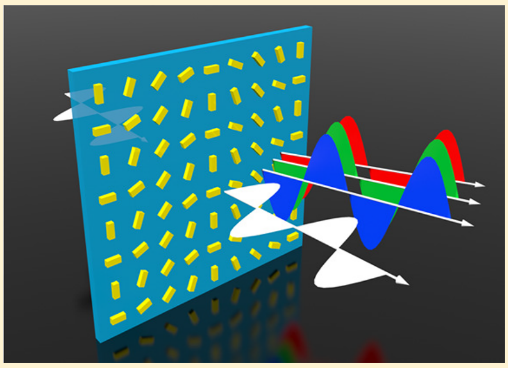

KEYWORDS: *plasmonic metasurface, wavelength-independent, refractive half-wave plate, single-layer*

Polarization is one of the intrinsic properties of electromagnetic waves and plays an important role in optical communication, computation, imaging, and display. Traditional methods of controlling the states of polarization usually involve bulky optical components like mirror, crystal, and prism that are infeasible for the miniaturization and integration of optical systems. Recently, metamaterials composed of arrays of various-shaped metallic or dielectric resonant structures have shown powerful ability in controlling the polarization states of light. Among them are arrays of planar single-layer and multilayer chiral metamolecules,[1−11] anisotropic resonators,[12−19] three-dimensional helix structures,[20,21] and localized surface plasmon (LSP) and surface plasmon polariton (SPP) based nanostructures.[22−26] Linear-to-circular polarization conversion or metasurface quarter-wave plate, has been accomplished by appropriately tailoring the transmission phases of the two orthogonal field components with different resonance frequencies.[25−27] $\pi/2$ phase difference and same amplitude at two orthogonal polarization directions generated by two principal axes guarantee that the scattered light is circularly polarized. Yu et al. proposed an alternative solution to make up a quart-wave plate by utilizing V-shaped antennas with varying distance between two set of elements, which causes the correct phase difference for the polarization of scattered light.[28−30] Pfeiffer et al. proposed the control of polarization by introducing multilayer metasurfaces with emergent functionalities;[31−34] the collective effect of reaction between layers provides a potential method to realize the polarization manipulation. Besides, metasurfaces with rotated nanoantennas have also exhibited the capability of splitting purely circularly polarized light from any polarized incident light.[35−37]

Metasurface half-wave plates, however, seem to be more challenging to realize because of the difficulties in finding the phase difference of π in two orthogonal polarization directions. Pors et al. proposed a reflective metasurface half-wave plate consisting of nanopatches and gold ground mirror.[38] The coupling between the metallic ground plane and the nanopatches in such designs increases the phase difference to π between the two orthogonal polarization directions.[39,40] Another type of metasurface half-wave plate is based on the polarization conversion for linearly polarized (LP) light.[29,31,41,42] The incident polarization will be partially converted to the orthogonal direction by the asymmetric geometry of optical antennas such as V-shaped and L-shaped antennas. Chen et al. proposed few-layer metasurface structures to improve the efficiency of linear polarization conversion operating either in transmission or in reflection mode.[43] But the

Received: May 16, 2017
Published: June 30, 2017

DOI: 10.1021/acsphotonics.7b00491
ACS Photonics XXXX, XXX, XXX−XXX

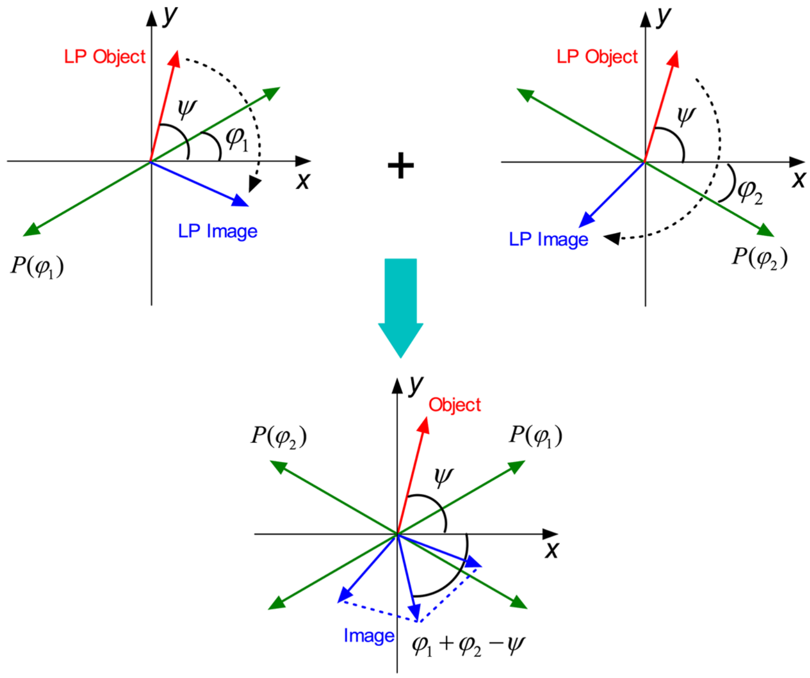

Figure 1. Geometry description of the polarization conversion process of our paired anisotropic nanoantennas. (Upper panel) $P(\varphi_1)$ and $P(\varphi_2)$ represent the anisotropic nanoantennas with orientation φ_1 and φ_2. Red arrows represent the polarization direction of the object light (or incident light) linearly polarized at angle ψ; blue arrows are the converted image light (or scattered light) due to the nanoantennas $P(\varphi_{1,2})$, which are symmetric to the object polarization with respect to the orientation of antennas. (Bottom panel) The response of a nanoantenna pair. When two antennas are added together, object light will be transformed to the image light polarized at $\varphi_1 + \varphi_2 - \psi$, which is the vector superposition of the individual images and is symmetric to the object with respect to the bisector of two nanoantennas.

aforementioned metasurface half-wave plates either operate in reflection or only permit conversion for linearly polarized incident light with a fixed polarization direction, limiting their practical applications in nano-optical systems. Arbabi et al. reported a class of dielectric meta-molecule that can realize high-efficiency total-controlling of phase, intensity, and polarization, which is a new perspective to design polarization-related metasurface. However, this type of structure is strongly related to the physical properties and shape of the dielectric molecule and is difficult to applicate in other frequency regime.[44]

Here, we propose a general idea to design a metasurface half-wave plate that can apply to any structure, material, and wavelength; The function of these class of half-wave plates is like that of the traditional half-wave plate changing the polarization angle from θ to $-\theta$ with respect to the optical axis for any polarizations. We then present a single-layer refractive metasurface half-wave plates based on our theory, whose optical axis and polarization conversion effect are accomplished through appropriately varying the orientation of the metallic nanorods. The conversion angle of our designing is wavelength-independent, meaning the polarization of scattered light maintains the same if incident polarization is fixed even if the wavelength is varied. Rigorous theoretic analysis and experiment demonstration indicate that our metasurface half-wave plates contain the same function and symmetry properties as in a classical half-wave plate. Because the presented metasurface half-wave plates do not require resonance of plasmonic eigenmodes, the orientation and quality of converted polarization can be maintained well not only on single wavelength at resonance frequency, but also over a bandwidth where the unit particle has a response to the incident light. This approach can also be easily generalized to other metasurface structures and wavelengths from visible light to microwaves.

■ THEORETICAL ANALYSIS ON THE OPTICAL ACTIVITY OF ANISOTROPIC NANOANTENNAS

To freely design the single-layer refractive metasurface half-wave plates, we first propose the theoretical analysis on the optical activity of anisotropic nanoantennas. Anisotropic nanoantennas have distinct optical responses for incident light linearly polarized in the two orthogonal directions. The mirror effect we proposed here is an alternative description of anisotropic nanoantennas in the presentation of circular polarizations. We denote left circularly polarized (LCP) and right circularly polarized (RCP) light as $|L\rangle = \begin{bmatrix} 1 \\ -i \end{bmatrix}$ and $|R\rangle = \begin{bmatrix} 1 \\ i \end{bmatrix}$, where the entries in the vector represent the complex amplitude in the x and y direction, respectively. The total transmission process for LCP and RCP incident lights can be discribed as[35,45−47]

$$P(\varphi)|L\rangle = \alpha|L\rangle + \beta|R\rangle e^{-i2\varphi} \tag{1}$$

$$P(\varphi)|R\rangle = \alpha|R\rangle + \beta|L\rangle e^{i2\varphi} \tag{2}$$

where φ is the polarizing direction (or orientation) of the nanoantenna, and α and β are the transmission amplitudes with $\alpha + \beta = 1$ after normalization. For LCP incident light, part of it will be converted into RCP light with an additional phase of -2φ. Unlike conventional optical elements that introduce phase changes through optical path differences, the additional phase here is induced by the Pancharatnam−Berry geometric phase.[48,49] Specifically, when the polarization of a beam traverses a closed loop on the Poincare sphere, the final state

DOI: 10.1021/acsphotonics.7b00491
ACS Photonics XXXX, XXX, XXX−XXX

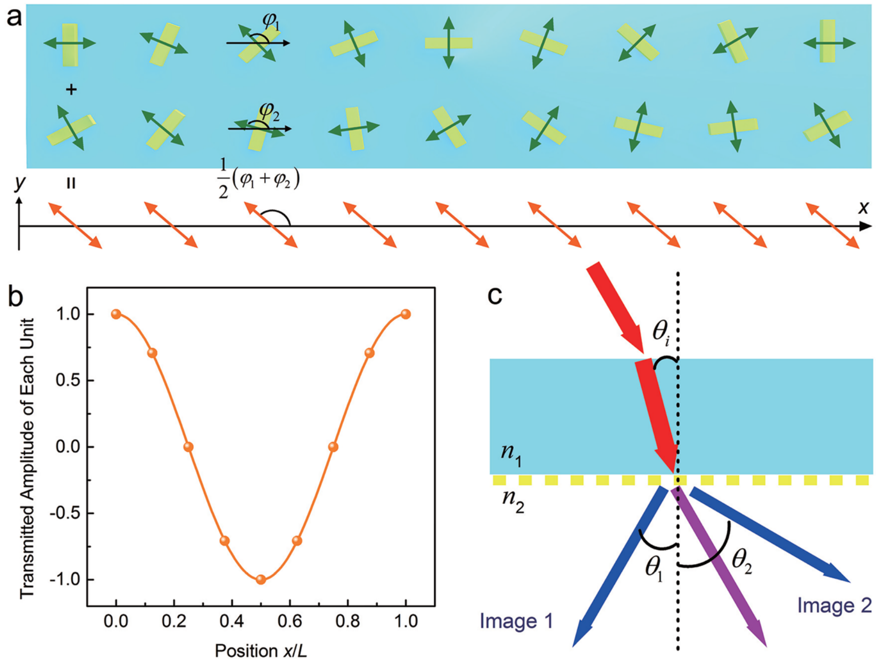

Figure 2. Schematic illustration of metasurface half-wave plate. (a) Arrangement of anisotropic metal nanoantenna pairs forming a superunit cell. The top row nanoantennas rotate in the clockwise direction, while the bottom row nanoantennas rotate in the counterclockwise direction. The green arrows indicate the polarizing direction of the individual nanoantenna, and the orange arrows show the bisection angle of the nanoantenna pairs $(\varphi_1 + \varphi_2)/2$, that is, the optical axis of the metasurface. (b) The transmission amplitude of the image light within the superunit-cell as a function of position. (c) Schematic illustration of the different propagation directions of the object (purple) and image (blue) light caused by the amplitude modulation in the metasurface.

differs from the initial state by a phase factor equal to half of the area which is encompassed by the loop on the sphere. For linearly polarized (LP) light, the mirror effect of the anisotropic nanoantenna can be derived by implementing eqs 1 and 2, from which we obtain

$$P(\varphi)|\mathrm{LP}\rangle_\psi = P(\varphi)\left[\frac{1}{2}e^{i\psi}|L\rangle + \frac{1}{2}e^{-i\psi}|R\rangle\right] = \alpha|\mathrm{LP}\rangle_\psi + \beta|\mathrm{LP}\rangle_{2\varphi-\psi} \tag{3}$$

where $|\mathrm{LP}\rangle_\psi$ denotes linearly polarized light with a polarization angle ψ, and has the expression of $|\mathrm{LP}\rangle_\psi = \begin{bmatrix}\cos\psi\\ \sin\psi\end{bmatrix}$. Equation 3 indicates that the outgoing light has two linear polarization components: one maintaining its polarization angle and the other rotating its polarization angle to $2\varphi - \psi$. These two polarization angles have mirror symmetry with respect to the nanoantenna orientation φ, so we denote $|\mathrm{LP}\rangle_\psi$ the object with amplitude α and $|\mathrm{LP}\rangle_{2\varphi-\psi}$ the image with amplitude β.

Based on this property of anisotropic nanoantenna, in the following we describe the design of a half-wave plate consisting of nanoantennas pairs schematically shown in Figure 1. The first nanoantenna has its orientation angle φ_1 with respect to the x-axis, where the object light polarized along the red arrow direction (upper-left panel in Figure 1) is partially converted to image light polarized along the blue arrow direction. The second nanoantenna is orientated at φ_2 with respect to the x-axis, resulting in image light polarized along the blue arrow direction shown in the upper-right panel of Figure 1. If we combine these two nanoantennas forming a nanoantenna pair, we can find that the expression for the final polarization state is

$$[P(\varphi_1) + P(\varphi_2)]|\mathrm{LP}\rangle_\psi = \alpha|\mathrm{LP}\rangle_\psi + \beta\cos(\varphi_1 - \varphi_2)|\mathrm{LP}\rangle_{\varphi_1+\varphi_2-\psi} \tag{4}$$

The image light with a transmission amplitude β is linearly polarized at $\varphi_1 + \varphi_2 - \psi$ when the incident light is linearly polarized at ψ, and the image and object polarizations have mirror symmetry with respect to the bisector of two nanoantennas, as shown in the bottom panel of Figure 1. This indicates that an array of the nanoantenna pairs can function as a half-wave plate, with the optical axis at $(\varphi_1 + \varphi_2)/2$ for linearly polarized incident light. Strict derivation shows that the electric field of output light forms a Jones vector for incident light with arbitrary polarization (see Supporting Information):

$$|E_{\mathrm{out}}\rangle = \alpha\begin{bmatrix}1 & 0\\ 0 & 1\end{bmatrix}|E_{\mathrm{in}}\rangle + \beta\cos(\varphi_1 - \varphi_2)\begin{bmatrix}\cos\Delta & \sin\Delta\\ \sin\Delta & -\cos\Delta\end{bmatrix}|E_{\mathrm{in}}\rangle \tag{5}$$

where $\Delta = \varphi_1 + \varphi_2$ is a newly introduced parameter for simplicity. The matrix in the second term represents a half-wave plate with the optical axis $\Delta/2$ with respect to the x-axis, and $\cos(\varphi_1 - \varphi_2)$ provides an additional amplitude modulation if we rotate the nanoantennas. As we can see from eq 5, the amplitudes of diffracted light are independent of the polarization of incident light, which means the efficiency of the proposed half-wave plate at fixed wavelength will be the same for any polarizations. Different from L- or V-shaped antennas that use resonant mode in particle to tune the phase and manipulate polarization of scattered light, our designing does not require any special physical property of antennas, and will not generate extra phase directly. It essentially utilizes Berry phase caused by rotation configuration and engineers the

DOI: 10.1021/acsphotonics.7b00491
ACS Photonics XXXX, XXX, XXX−XXX

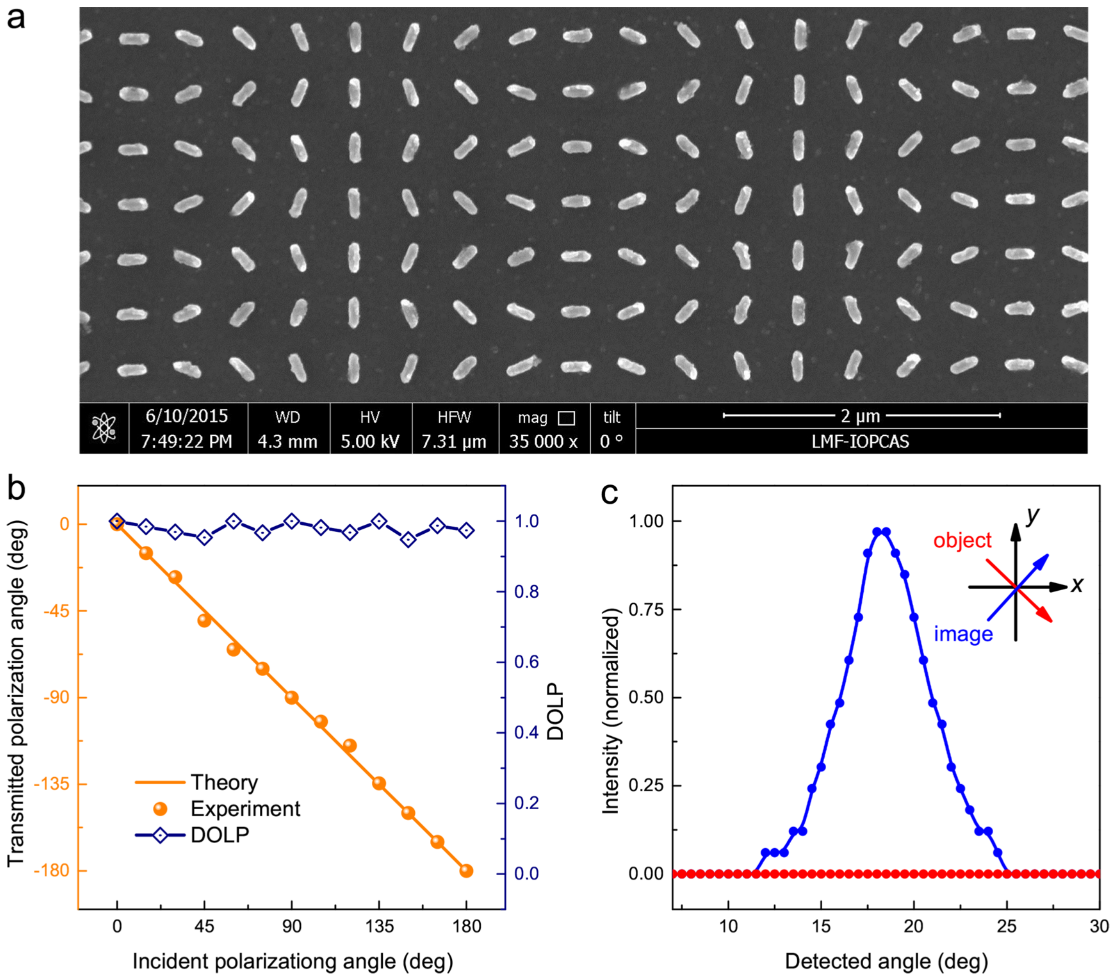

Figure 3. Experimental validation of metasurface functioning as a half-wave plate. (a) SEM image of the metasurface half-wave plate with optical axis along the x-axis; the nanoantenna has the length l = 200 nm, width w = 50 nm, and thickness t = 40 nm, and each nanoantenna pair maintains $\varphi_1 + \varphi_2 = 0$. (b) Polarization angle of the image light as a function of the polarization angle of the incident light at wavelength 980 nm. Orange symbols represent experimental measurements and the orange line indicates the behavior of a classical half-wave plate. The degree of linear polarization is given by the blue symbols at correspondent incident polarization angles. (c) Measured transmission intensity of the image light as a function of detection angle. The inset shows that the polarization angle is 135° for the incident light (object) and 45° for the image light. Blue and red symbols are results when analyzer angle was set to 45° and 135°, respectively.

scattered polarization directly with amplitude modulation $\beta \cos(\varphi_1 - \varphi_2)$.

In a uniform array of anisotropic nanoantenna pairs, the object and image beams (respectively the first and second terms in eq 5) propagate in the same direction. In order to create a half-wave plate, it is necessary to separate them so that they can propagate to different directions. For such a purpose, we introduce the linear rotation of a series of nanoantenna pairs forming a superunit-cell, as shown in Figure 2a. The nanoantennas in the first row within the superunit-cell rotate clockwise along the x-axis, while the nanoantennas in the second row rotate counterclockwise, with their principal polarizing axis indicated by the green arrows. The two nanoantennas in the same column form the nanoantenna pair. The angular bisector of the nanoantenna pairs remains constant during the rotation, which maintains the optical axis $\Delta/2 = (\varphi_1 + \varphi_2)/2$ of the half-wave plate. However, the transmission amplitude of the nanoantenna pairs is modulated by $\cos(\varphi_1 - \varphi_2)$, which varies along the x-direction, as shown in Figure 2b. According to eq 5, this extra variation of transmission amplitude provides a space frequency and alters the propagation direction of the transmitted image light just like in a sinusoidal amplitude diffraction grating. Exerting Fourier analysis on eq 5 shows that the transmitted image light is along two distinct angles θ_1 and θ_2, as shown in Figure 2c, given by

$$n_2 \sin \theta_{1,2} = n_1 \sin \theta_i \pm \frac{\lambda_0}{L} \tag{6}$$

where L is the period of the superunit-cell with nanoantennas rotating from 0 to π, λ_0 is the wavelength in vacuum, θ_i is the incident angle, and n_1 and n_2 are refractive indices in incident side and transmitted side, respectively. The two image beams have the same polarization states determined by the optical axis and incident polarization. For convenience, we set the incident angle $\theta_i = 0°$ in the following discussions.

EXPERIMENTAL DEMONSTRATION OF METASURFACE HALF-WAVE PLATE

To validate the feasibility of the theoretical proposal, we adopted nanorod, which can be viewed as dipole, as our basic anisotropic element. At resonant frequency, the current driven in the rod causes large reflection and absorption for the linearly

DOI: 10.1021/acsphotonics.7b00491
ACS Photonics XXXX, XXX, XXX−XXX

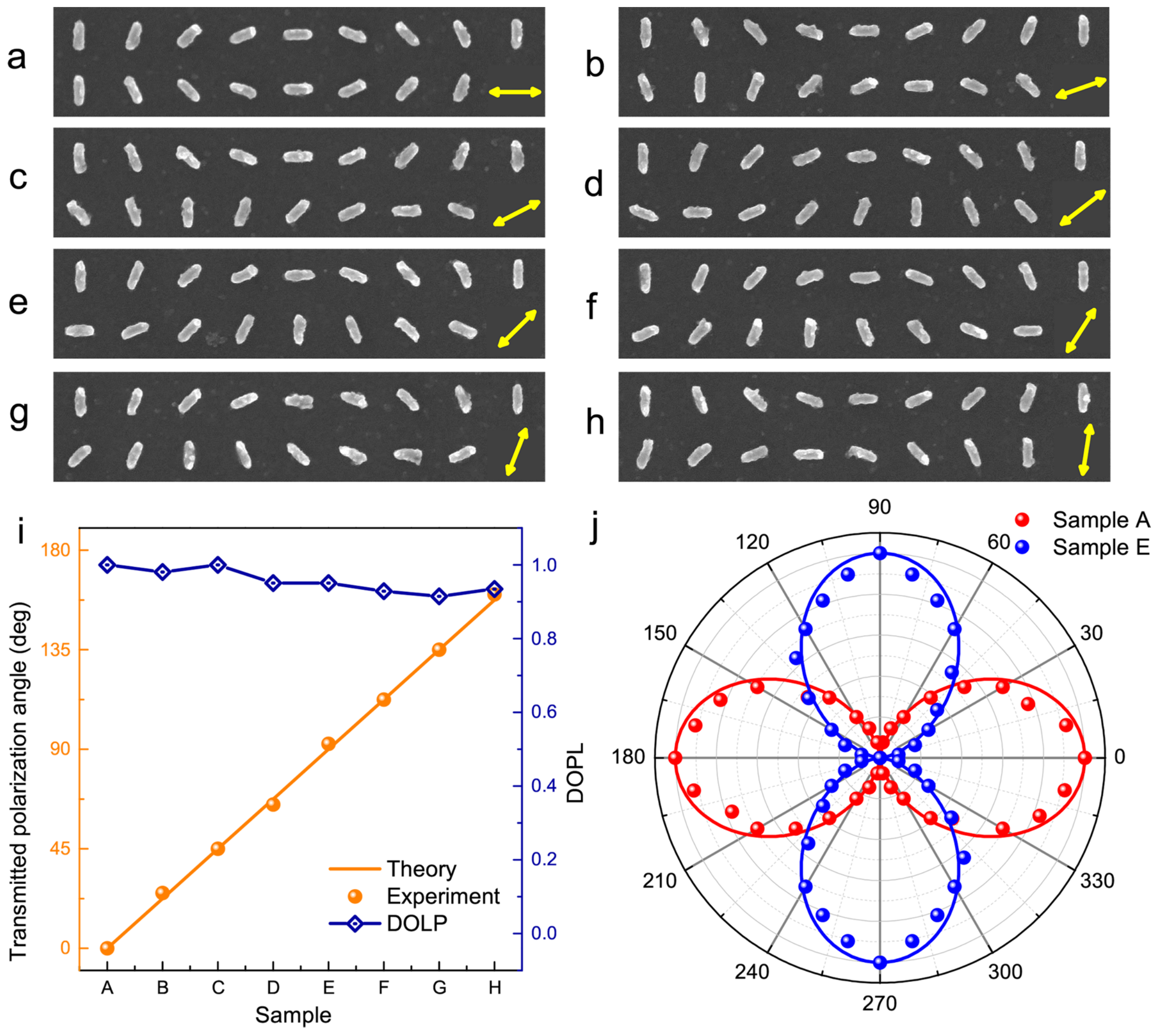

Figure 4. Optical axis of the metasurface half-wave plates. (a−h) SEM images of samples A−H, where the optical axis varies from 0° to 78.75° at intervals of 11.25°. The arrow in the right corner of each sample indicates the orientation of the optical axis. (i) Experimentally measured (orange symbols) and theoretically predicted (orange line) polarization angle of the image light when the incident light is linearly polarized at 0° for samples A−H. The degree of linear polarization (DOLP) is illustrated by the blue symbols. (j) Results of state-of-polarization analysis for samples A (red) and E (blue) by measuring the transmission intensity after rotating the analyzer from 0° to 360°. Experimental results are given by the symbols and the curves are obtained from analytical calculations.

polarized light with polarization along with the rod. Weak coupling will also diminish the transmission light. For the polarization perpendicular to the rod, incident light will not be affected due to the high-frequency resonance. This is the mechanism of the anisotropic property of nanorod. We fabricated metasurfaces half-wave plate consisting of gold nanorods on a glass substrate with length l = 200 nm, width w = 50 nm, and thickness t = 40 nm. Electron-beam lithography, metal evaporation, and lift-off process were used to fabricate the metallic structures. Quartz substrates were first cleaned and evaporated of 5 nm Cr film as conductive layer for the following e-beam lithography. Then PMMA resist was spin-coated onto the substrate and baked on a hot plate for 1 min. The nanorod patterns were formed by e-beam lithography system (JBX-6300FS) at 100 keV to reduce the proximity effect. The 40 nm Au film was deposited onto the samples, followed by lift-off process in acetone to get Au patterns. The Cr layer can be removed in $Ce(NH_4)_4(NO_3)_6$/acetic acid solution for 30 s, which should be well controlled to avoid excessive removal of Cr below the metal patterns. The size of each pattern array is 300 × 300 μm^2.

As the incident light is circularly polarized light, the gold dipole will convert part of the light to the opposite polarization with conversion efficiency dependent on wavelength (see Figure S3 in Supporting Information). Eight nanorod pairs constitute the superunit-cell with a period L = 2400 nm, where the orientation of nanorods rotates with an angle increment of $\pi/8$ either clockwise or counterclockwise, as shown in the SEM image in Figure 3a.The nanorod pairs are arranged so that the optical axis is along the x-axis, that is, $(\varphi_1 + \varphi_2)/2 = 0°$.

The experiments were carried out using a custom-built optical setup (see Supporting Information). Semiconductor lasers were used to provide laser pulses with a central wavelength of either 900 or 980 nm. An aperture was used to adjust the spot diameter. A polarizer was applied to purify the linear polarization of the incident light, which was focused on the sample with a 20×/0.40 NIR microscope objective. For the refractive detection, we used a concentric rotation system to achieve independent rotations of the sample orientation and the detection angle. The resolution of the rotation system was 0.02°. One of the rotation stages was used to adjust the sample orientation for normal incidence. The intensity, polarization

DOI: 10.1021/acsphotonics.7b00491
ACS Photonics XXXX, XXX, XXX−XXX

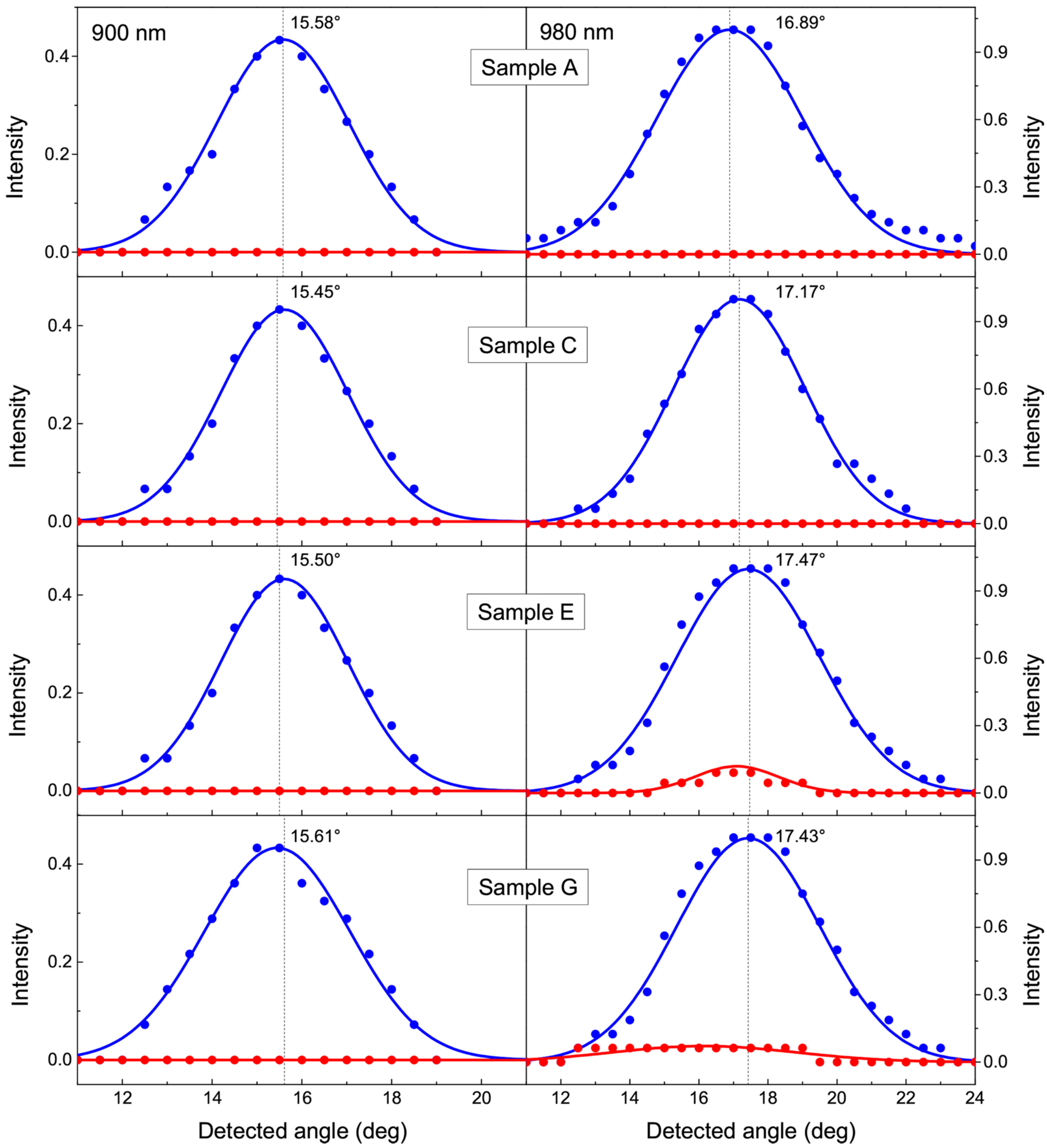

Figure 5. Wavelength-independent operation of the metasurface half-wave plates. Intensity of the transmitted image light was measured as a function of detection angle at wavelengths 900 and 980 nm, with the analyzer aligned with the expected polarization direction (blue symbols) and its orthogonal direction (red symbols). All the intensities are normalized to the maximum intensity in 980 nm. The peak value, representing the diffraction angle, are about 15° and 17° for 900 and 980 nm cases, respectively, consistent with prediction of eq 6. The measurements were performed under normal incidence. Solid curves are Gaussian fit of the experimental data.

state, and transmission angle of the image light were measured using a combination of a lens, an analyzer, and a power meter in the rotation system. All of the optical elements, including the microscope objective, lens, polarizer, and detector, operate in the broadband near-infrared wavelength range. Since the two diffracted lights from our sample have same polarization property in theory and same characteristic in experiments, we only analyzed one of the diffracted light for simplicity.

Figure 3b presents the polarization angle of the transmitted light and the degree of linear polarization (DOLP) when the polarization angle of the incident light varies from 0 to π at the wavelength 980 nm. The experimentally measured polarization angles (orange symbols) are compared with the theoretical prediction (orange line) of a classical half-wave plate with its optical axis also along the x-axis. The experiment results are in excellent agreement with the prediction as well as the theoretical analysis presented by eq 4. The quality of linear polarization of the transmitted image light is represented by the DOLP which is defined as DOLP = $1 - I_{min}/I_{max}$, where I_{min} and I_{max} are, respectively, the minimum and maximum intensities of the image light after propagating across an analyzer. The experimentally measured DOLP is illustrated by the blue symbols in Figure 3b, exhibiting values close to 1 for all incident polarization angles. This is expected as the image light has been split from the object light by introducing the sinusoidal modulation of intensity as in eq 4. When the incident light is polarized at 135°, we plot in Figure 3c the detected intensity of the image light as a function of detection angle after it passes through an analyzer. In our experiments, the incident light is cast from glass (n_1 = 1.5) to air (n_2 = 1). When the angle

DOI: 10.1021/acsphotonics.7b00491
ACS Photonics XXXX, XXX, XXX−XXX

of the analyzer is 45°, the transmission is peaked at 17.8°, consistent with the prediction in eqs 4 and 6; while the angle of the analyzer is set to 135°, there is hardly detectable transmission. The detection angle dependent transmission intensity profile in our experiments has a relatively large full width at half-maximum (fwhm), which is caused by the small size of our sample as compared to the width of the incident Gaussian beam (see Supporting Information).

We carried out additional experiments to further verify that the optical axis is determined by the angular bisector $(\varphi_1 + \varphi_2)/2$ of the nanoantenna pairs, through measuring the polarization angle and DOLP in a series of metasurfaces with different $(\varphi_1 + \varphi_2)/2$. Figure 4a–h shows SEM images of eight metasurface half-wave plate samples (named samples A–H, respectively), where the angular bisector of the nanoantenna pairs $(\varphi_1 + \varphi_2)/2$ varies from 0° to 78.75° with an increment of 11.25°, while the structural parameters are otherwise the same. The orange symbols in Figure 4I show the detected polarization angles of the image light when the incident light is linearly polarized at 0°, together with the predictions of classical half-wave plates with the correspondent optical axes (orange line). The excellent agreement proves that the bisector of the nanoantenna pairs $(\varphi_1 + \varphi_2)/2$ solely determines the optical axis of the metasurface half-wave plates. The high DOLP of the transmitted image light is also maintained, as shown by the blue symbols in Figure 4i. State-of-polarization analysis is shown in Figure 4j for sample A with optical axis angle 0° (red symbols) and sample E with optical axis angle 45° (blue symbols), which were carried out by measuring the intensity of the image light after rotating the analyzer. The red and blue curves are obtained from analytical calculations for linearly polarized light with polarization angles of 0° and 90°, respectively. The good correspondence suggests again that the transmitted image light is linearly polarized with high quality, with the polarization angle determined by both the polarization angle of the incident light and the optical axis of the metasurface half-wave plate.

Our metasurface half-wave plates have the same symmetry characteristics as in classical half-wave plates. For example, sample C has its optical axis at 22.5° and sample G 67.5°, and their distribution of nanorods is symmetrical to each other about x- or y-axis. If we flip sample C with respect to either x- or y-axis, it will become sample G. Hence, samples C and G behave the same if the incident light is cast from the glass substrate side for the former and the air side for the latter. Similarly, samples B and H and samples D and F are also symmetrical to each other with respect to x- or y-axis, and samples A and E are self-symmetrical (see Supporting Information).

Our metasurfaces realize the half-wave plate functionality based on the arrangement of nanoantennas and they rely very little on the nanoantenna resonance. Therefore, their conversion performance can be maintained when the wavelength of the incident light departs from the nanoantenna resonance, which only affects the scattering coefficient β and, therefore, the efficiency of the image light according to eq 5. Thus, our metasurfaces can perform as half-wave plates over a relatively wide wavelength range with high DOLP even if the efficiency is not as high as resonance wavelength. To prove this feature, we measured the transmission of the image light in samples A, C, E, and G at wavelengths 900 and 980 nm. The experimental results are shown in Figure 5, where the incident polarization angle was set to 0°, and the intensity of the image light was detected as a function of detection angle when the analyzer was aligned with the theoretically predicted polarization direction (blue curves) and its orthogonal direction (red curves). Despite the difference of total intensities and transmission angles determined by eq 6, the four samples function well and have high values of DOLP at both 900 and 980 nm, revealing the wave-independent operation of the metasurface half-wave plates. The minor component in orthogonal polarization for the sample E at 980 nm incidence, however, might be caused by either imperfect linearized polarization of incident light or imperfect fabrication. The inaccurate period in samples will deflect object light into the direction with scattered image light and induce the orthogonal component. The efficiency of the proposed metasurface (as indicated by eq 5) can be expressed by the square of conversion coefficient β. The maximum value of the conversion coefficient β is about 0.44 at 980 nm (see Figure S3 in Supporting Information). However, as the converted lights are split into two bunches, only half of the expected efficiency can be achieved. The efficiency can be definitely improved by replacement of the nanorods to the other more efficient unit. Theoretically, the maximum efficiency of the polarization conversion of our antenna-rotation configuration can be reached 50% if shape and material of antennas are properly chosen.

■ DISCUSSIONS AND CONCLUSIONS

The presented metasurface half-wave plates, unlike other metasurface-based "half-wave plates" that only support cross-polarization conversion with incident light polarized at a specific direction, can be used as real half-wave plates realizing full functionality. In the present work, we chose gold nanorod as the anisotropic optical antenna to realize metasurface half-wave plates, which demonstrates the perfect polarization conversion in a wavelength-independent way. The propagation direction of image light is different from the ordinary transmission direction and depends on the wavelength as well as the period of the superunit-cell. From the point of view of serving as a half-wave plate, this might be considered as a disadvantage because some additional optical components are necessary to align the optical path. We cannot simply tune the polarization by solely rotating the sample, since the diffracted light will spatially change its propagating direction as well (though the polarization is changed as desired). It is more pratical to be designed as a bespoke device for specific situation. However, it can be also advantageous as the scattering angle of the image beams can be changed by properly tuning the period of the superunit-cell. This would make it possible to construct multifunctional photonic devices with simultaneous polarization and wavefront controls. Additionally, although we only show the designing in optical regime, our theory can apply to any other electromagnetism wavelengths, especially in Terahertz, where only limited optical elements are available. Beyond our most common prototype with gold nanorods, optimization of the performance is quite possible by changing the materials and shape of nanostructure. Anyway, our theory indicates a generalized method in designing polarization controlling system far beyond traditional optical elements. Our designing has promising applications in photonic device minimization, Terahertz optics, imaging, and any field with polarization control.

In conclusion, based on the mirror effect of anisotropic optical antennas, we theoretically proposed and experimentally

DOI: 10.1021/acsphotonics.7b00491
ACS Photonics XXXX, XXX, XXX–XXX

validated metasurface half-wave plates whose optics axis is determined by the bisection angle of counter-rotated nanoantenna pairs. The intensity modulated scattering enables us to split the useful converted image light from the object light, and the image beams have a good degree of linear polarization (in case of linearly polarized incident light) at the direction exactly predicted by a classical half-wave plate. The metasurface half-wave plates do not rely on the resonant response of the nanoantennas, and can produce high degree of linear polarized transmitted light not only on single resonance wavelength but also over the spectrum where nanoparticles have response to incident light. We verified the easy-implemented configuration using nanorods metasurface. One can easily adopt other unit particles with high efficiency and replace the nanorod with them. This work suggests more degrees of freedom in accomplishing broadband multifunctional photonic devices for polarization control, wavefront engineering, and beam forming.

■ ASSOCIATED CONTENT

Ⓢ Supporting Information

The Supporting Information is available free of charge on the ACS Publications website at DOI: 10.1021/acsphotonics.7b00491.

> The theoretical formulation on the plasmonic half-wave plates, the polarization conversion of sample E, the analysis of state-of-polarization of all samples, the bandwidth of the metasurface half-wave plates, the experimental manifestation of symmetrical property and a schematic configuration of the experimental setup (PDF).

■ AUTHOR INFORMATION

Corresponding Author

*E-mail: schen@nankai.edu.cn.

ORCID

Junjie Li: 0000-0002-1508-9891

Hou-Tong Chen: 0000-0003-2014-7571

Shuqi Chen: 0000-0002-7898-4148

Author Contributions

†Z.Liu and Z.Li contributed equally to this work.

Notes

The authors declare no competing financial interest.

■ ACKNOWLEDGMENTS

This work was supported by the National Key Research and Development Program of China (2016YFA0301102), the Natural Science Foundation of China (11574163 and 61378006), and the Program for New Century Excellent Talents in University (NCET-13-0294). We also acknowledge the support from the Collaborative Innovation Center of Extreme Optics, Shanxi University, Taiyuan, Shanxi 030006, China.

■ REFERENCES

(1) Prosvirnin, S. L.; Zheludev, N. I. Polarization effects in the diffraction of light by a planar chiral structure. *Phys. Rev. E* **2005**, *71*, 037603.

(2) Papakostas, A.; Potts, A.; Bagnall, D. M.; Prosvirnin, S. L.; Coles, H. J.; Zheludev, N. I. Optical Manifestations of Planar Chirality. *Phys. Rev. Lett.* **2003**, *90*, 107404.

(3) Plum, E.; Zhou, J.; Dong, J.; Fedotov, V. A.; Koschny, T.; Soukoulis, C. M.; Zheludev, N. I. Metamaterial with negative index due to chirality. *Phys. Rev. B: Condens. Matter Mater. Phys.* **2009**, *79*, 035407.

(4) Xiong, X.; Sun, W.-H.; Bao, Y.-J.; Wang, M.; Peng, R.-W.; Sun, C.; Lu, X.; Shao, J.; Li, Z.-F.; Ming, N.-B. Construction of a chiral metamaterial with a U-shaped resonator assembly. *Phys. Rev. B: Condens. Matter Mater. Phys.* **2010**, *81*, 075119.

(5) Decker, M.; Zhao, R.; Soukoulis, C. M.; Linden, S.; Wegener, M. Twisted split-ring-resonator photonic metamaterial with huge optical activity. *Opt. Lett.* **2010**, *35*, 1593−1595.

(6) Svirko, Y.; Zheludev, N.; Osipov, M. Layered chiral metallic microstructures with inductive coupling. *Appl. Phys. Lett.* **2001**, *78*, 498−500.

(7) Zhao, Y.; Belkin, M. A.; Alù, A. Twisted optical metamaterials for planarized ultrathin broadband circular polarizers. *Nat. Commun.* **2012**, *3*, 870.

(8) Xu, H.; Wang, G. M.; Qi, M. Q.; Cai, T.; Cui, T. J. Compact dual-band circular polarizer using twisted Hilbert-shaped chiral metamaterial. *Opt. Express* **2013**, *21*, 24912−24921.

(9) Cong, L.; Xu, N.; Han, J.; Zhang, W.; Singh, R. A Tunable Dispersion-Free Terahertz Metadevice with Pancharatnam-Berry-Phase-Enabled Modulation and Polarization Control. *Adv. Mater.* **2015**, *27*, 6630−6636.

(10) Cong, L.; Srivastava, Y. K.; Singh, R. Near-Field Inductive Coupling Induced Polarization Control in Metasurfaces. *Adv. Opt. Mater.* **2016**, *4*, 848−852.

(11) Cong, L.; Srivastava, Y. K.; Singh, R. Inter and intra-metamolecular interaction enabled broadband high-efficiency polarization control in metasurfaces. *Appl. Phys. Lett.* **2016**, *108*, 011110.

(12) Pfeiffer, C.; Zhang, C.; Ray, V.; Guo, L. J.; Grbic, A. Polarization rotation with ultra-thin bianisotropic metasurfaces. *Optica* **2016**, *3*, 427−432.

(13) Kruk, S.; Hopkins, B.; Kravchenko, I. I.; Miroshnichenko, A.; Neshev, D. N.; Kivshar, Y. S. Invited Article: Broadband highly efficient dielectric metadevices for polarization control. *APL Photon.* **2016**, *1*, 030801.

(14) Li, Z.; Liu, W.; Cheng, H.; Chen, S.; Tian, J. Realizing broadband and invertible linear-to-circular polarization converter with ultrathin single-layer metasurface. *Sci. Rep.* **2016**, *5*, 18106.

(15) Biagioni, P.; Savoini, M.; Huang, J. S.; Duo, L.; Finazzi, M.; Hecht, B. Near-field polarization shaping by a near-resonant plasmonic cross antenna. *Phys. Rev. B: Condens. Matter Mater. Phys.* **2009**, *80*, 153409.

(16) Strikwerda, A. C.; Fan, K.; Tao, H.; Pilon, D. V.; Zhang, X.; Averitt, R. D. Comparison of birefringent electric split-ring resonator and meanderline. *Opt. Express* **2009**, *17*, 136−149.

(17) Peralta, X. G.; Smirnova, E. I.; Azad, A. K.; Chen, H.-T.; Taylor, A. J.; Brener, I.; O'Hara, J. F. Metamaterials for THz polarimetric devices. *Opt. Express* **2009**, *17*, 773−783.

(18) Li, J.; Chen, S.; Yang, H.; Li, J.; Yu, P.; Cheng, H.; Gu, C.; Chen, H.-T.; Tian, J. Simultaneous control of light polarization and phase distributions using plasmonic metasurfaces. *Adv. Funct. Mater.* **2015**, *25*, 704−710.

(19) Ma, H. F.; Tang, W. X.; Cheng, Q.; Cui, T. J. A single metamaterial plate as bandpass filter, transparent wall, and polarization converter controlled by polarizations. *Appl. Phys. Lett.* **2014**, *105*, 081908.

(20) Zhang, S.; Park, Y. S.; Li, J.; Lu, X.; Zhang, W.; Zhang, X. Negative refractive index in chiral metamaterials. *Phys. Rev. Lett.* **2009**, *102*, 023901.

(21) Gansel, J. K.; Thiel, M.; Rill, M. S.; Decker, M.; Bade, K.; Saile, V.; Freymann, G.; Linden, S.; Wegener, M. Gold helix photonic metamaterial as broadband circular polarizer. *Science* **2009**, *325*, 1513−1515.

(22) Li, T.; Wang, S. M.; Cao, J. X.; Liu, H.; Zhu, S. N. Cavity-involved plasmonic metamaterial for optical polarization conversion. *Appl. Phys. Lett.* **2010**, *97*, 261113.

(23) Li, T.; Liu, H.; Wang, S. M.; Yin, X. G.; Wang, F. M.; Zhu, S. N.; Zhang, X. Manipulating optical rotation in extraordinary transmission by hybrid plasmonic excitations. *Appl. Phys. Lett.* **2008**, *93*, 021110.

(24) Wu, S.; Zhang, Z.; Zhang, Y.; Zhang, K.; Zhou, L.; Zhang, X.; Zhu, Y. Enhanced rotation of the polarization of a light beam transmitted through a silver film with an array of perforated S-shaped holes. *Phys. Rev. Lett.* **2013**, *110*, 207401.
(25) Khoo, E. H.; Li, E. P.; Crozier, K. B. Plasmonic wave plate based on subwavelength nanoslits. *Opt. Lett.* **2011**, *36*, 2498−2500.
(26) Zhao, Y.; Alù, A. Tailoring the dispersion of plasmonic nanorods to realize broadband optical meta-waveplates. *Nano Lett.* **2013**, *13*, 1086−1091.
(27) Roberts, A.; Lin, L. Plasmonic quarter-wave plate. *Opt. Lett.* **2012**, *37*, 1820−1822.
(28) Yu, N.; Aieta, F.; Genevet, P.; Kats, M. A.; Gaburro, Z.; Capasso, F. A broadband, background-free quarter-wave plate based on plasmonic metasurfaces. *Nano Lett.* **2012**, *12*, 6328−6333.
(29) Yu, N.; Genevet, P.; Kats, M. A.; Aieta, F.; Tetienne, J. P.; Capasso, F.; Gaburro, Z. Light propagation with phase discontinuities: generalized laws of reflection and refraction. *Science* **2011**, *334*, 333−337.
(30) Yu, N.; Capasso, F. Flat optics with designer metasurfaces. *Nat. Mater.* **2014**, *13*, 139−150.
(31) Pfeiffer, C.; Emani, N. K.; Shaltout, A. M.; Boltasseva, A.; Shalaev, V. M.; Grbic, A. Efficient light bending with isotropic metamaterial Huygens' surfaces. *Nano Lett.* **2014**, *14*, 2491−2497.
(32) Pfeiffer, C.; Grbic, A. Cascaded metasurfaces for complete phase and polarization control. *Appl. Phys. Lett.* **2013**, *102*, 231116.
(33) Monticone, F.; Estakhri, N. M.; Alù, A. Full control of nanoscale optical transmission with a composite metascreen. *Phys. Rev. Lett.* **2013**, *110*, 203903.
(34) Cheng, H.; Liu, Z.; Chen, S.; Tian, J. Emergent Functionality and Controllability in Few-Layer Metasurfaces. *Adv. Mater.* **2015**, *27*, 5410−5421.
(35) Huang, L.; Chen, X.; Mühlenbernd, H.; Li, G.; Bai, B.; Tan, Q.; Jin, G.; Zentgraf, T.; Zhang, S. Dispersionless phase discontinuities for controlling light propagation. *Nano Lett.* **2012**, *12*, 5750−5755.
(36) Chen, X.; Huang, L.; Mühlenbernd, H.; Li, G.; Bai, B.; Tan, Q.; Jin, G.; Qiu, C. W.; Zhang, S.; Zentgraf, T. Dual-polarity plasmonic metalens for visible light. *Nat. Commun.* **2012**, *3*, 1198.
(37) Liu, Z.; Li, Z.; Liu, Z.; Li, J.; Cheng, H.; Yu, P.; Liu, W.; Tang, C.; Gu, C.; Li, J.; Chen, S.; Tian, J. High-Performance Broadband Circularly Polarized Beam Deflector by Mirror Effect of Multinanorod Metasurfaces. *Adv. Funct. Mater.* **2015**, *25*, 5428−5434.
(38) Pors, A.; Nielsen, M. G.; Bozhevolnyi, S. I. Broadband plasmonic half-wave plates in reflection. *Opt. Lett.* **2013**, *38*, 513−515.
(39) Ding, F.; Wang, Z.; He, S.; Shalaev, V. M.; Kildishev, A. V. Broadband high-efficiency half-wave plate: a supercell-based plasmonic metasurface approach. *ACS Nano* **2015**, *9*, 4111−4119.
(40) Shaltout, A.; Liu, J.; Kildishev, A.; Shalaev, V. Photonic spin Hall effect in gap-plasmon metasurfaces for on-chip chiroptical spectroscopy. *Optica* **2015**, *2*, 860−863.
(41) Li, Z.; Chen, S.; Tang, C.; Liu, W.; Cheng, H.; Liu, Z.; Li, J.; Yu, P.; Xie, B.; Liu, Z.; Li, J.; Tian, J. Broadband diodelike asymmetric transmission of linearly polarized light in ultrathin hybrid metamaterial. *Appl. Phys. Lett.* **2014**, *105*, 201103.
(42) Liu, W.; Chen, S.; Li, Z.; Cheng, H.; Yu, P.; Li, J.; Tian, J. Realization of broadband cross-polarization conversion in transmission mode in the terahertz region using a single-layer metasurface. *Opt. Lett.* **2015**, *40*, 3185−3188.
(43) Grady, N. K.; Heyes, J. E.; Chowdhury, D. R.; Zeng, Y.; Reiten, M. T.; Azad, A. K.; Taylor, A. J.; Dalvit, D. A. R.; Chen, H.-T. Terahertz metamaterials for linear polarization conversion and anomalous refraction. *Science* **2013**, *340*, 1304−1307.
(44) Arbabi, A.; Horie, Y.; Bagheri, M.; Faraon, A. Dielectric metasurfaces for complete control of phase and polarization with subwavelength spatial resolution and high transmission. *Nat. Nanotechnol.* **2015**, *10*, 937−943.
(45) Liu, Z.; Chen, S.; Li, J.; Cheng, H.; Li, Z.; Liu, W.; Yu, P.; Xia, J.; Tian, J. Fully interferometric controllable anomalous refraction efficiency using cross modulation with plasmonic metasurfaces. *Opt. Lett.* **2014**, *39*, 6763−6766.
(46) Gori, F. Measuring Stokes parameters by means of a polarization grating. *Opt. Lett.* **1999**, *24*, 584−586.
(47) Bomzon, Z. E.; Biener, G.; Kleiner, V.; Hasman, E. Space-variant Pancharatnam-Berry phase optical elements with computer-generated subwavelength gratings. *Opt. Lett.* **2002**, *27*, 1141−1143.
(48) Shitrit, N.; Bretner, I.; Gorodetski, Y.; Kleiner, V.; Hasman, E. Optical spin Hall effects in plasmonic chains. *Nano Lett.* **2011**, *11*, 2038−2042.
(49) Shitrit, N.; Maayani, S.; Veksler, D.; Kleiner, V.; Hasman, E. Rashba-type plasmonic metasurface. *Opt. Lett.* **2013**, *38*, 4358−4361.

DOI: 10.1021/acsphotonics.7b00491
ACS Photonics XXXX, XXX, XXX−XXX